Journal of Molecular Spectroscopy 385 (2022) 111604

Contents lists available at ScienceDirect

Journal of Molecular Spectroscopy

journal homepage: www.elsevier.com/locate/yjmsp

Rotational spectrum of *anti*- and *gauche*-4-cyano-1-butyne (C_5H_5N) – An open-chain isomer of pyridine

P. Matisha Dorman [a], Brian J. Esselman [a], P. Bryan Changala [b], Samuel M. Kougias [a], Michael C. McCarthy [b,*], R. Claude Woods [a,*], Robert J. McMahon [a,*]

[a] Department of Chemistry, University of Wisconsin-Madison, 1101 University Avenue, Madison, WI 53706-1322, United States
[b] Center for Astrophysics, Harvard & Smithsonian, 60 Garden Street, Cambridge, MA 02138-1516, United States

ARTICLE INFO

Keywords:
Rotational spectroscopy
Microwave
Millimeter-wave
Astrochemistry
Centrifugal distorted rotor
Quadrupole coupling

ABSTRACT

The analysis of the rotational spectrum of 4-cyano-1-butyne, an open-chain isomer of pyridine, is presented herein for the first time. Transitions for the ground vibrational states of both conformational isomers, *anti* and *gauche*, were observed in the 8–38 GHz and 130–360 GHz frequency ranges and fit to effective sextic distorted-rotor Hamiltonians with low uncertainty (σ_{fit} < 50 kHz), allowing for their potential detection by radio-astronomy or in harsh reaction environments. The microwave region includes hyperfine-split transitions for both conformers, allowing for the experimental determination of the χ_{aa}, χ_{bb}, and χ_{cc} quadrupole coupling constants. In the millimeter-wave region, not every observable ground-state transition could be satisfactorily addressed by a single-state Hamiltonian due to Coriolis coupling with the low-energy vibrationally excited states. Thus, effective single-state fits of the ground states were obtained by including only K_a-series transitions without obviously perturbed energy levels. Importantly, the effective fit does include the most intense transitions throughout the observed frequency ranges. The predicted values (MP2/cc-pVTZ) are in close agreement with the experimental spectroscopic constants. These data provide a sufficient foundation for the identification of *anti*- and *gauche*-4-cyano-1-butyne in the interstellar medium by radioastronomy. The *gauche* conformer is estimated to lie 1.00 (5) kcal/mol higher in energy than the *anti* conformer, as determined using experimental transition intensities.

1. Introduction

Organic nitriles and isonitriles are well represented in the catalogue of >250 species detected in the interstellar medium (ISM) [1,2]. Because of the CN moiety, these groups typically have sizeable molecular dipole moments, resulting in intense rotational transitions detectable *via* radioastronomy. Recently, the first examples of five- and six-membered ring systems, ubiquitous in organic chemistry, were discovered in the ISM as their nitrile-substituted derivatives: benzonitrile [3], 1- and 2-cyanonaphthalene [4], and 1- and 2-cyano-1,3-cyclopentadiene [5,6]. These detections represent a dramatic advance in our understanding of interstellar organic chemistry, yet it remains unclear if these ring systems are formed through decomposition of larger polycyclic species or are generated from smaller precursors.

Computational and experimental studies of complex chemical reactions in the ISM are ongoing, and open-chain nitriles are emerging as attractive candidates for a possible mechanistic connection to aromatic species [7–9]. Combined with their prominent dipole moments (usually between 2 and 4 D), many nitriles possess observable hyperfine resolved transitions at low frequency that can also assist in their identification in the ISM. Open-chain nitriles of various chain lengths and levels of saturation have been detected in different regions of the ISM [10–21]. In a recent study, several open-chain nitriles and a few nitrile-substituted five- and six-membered rings were generated and detected in a benzene/nitrogen discharge [22]. Using spectral catalogues for known molecules, a complex mixture of many isomers with the same elemental formula were identified and assigned using microwave spectroscopy.

Organic nitriles and isonitriles have been of interest to our groups for some time due to their relevance to astrochemistry [3–5,23–27]. The Wisconsin group recently provided millimeter-wave rotational spectra of several pyridine (C_5H_5N) isomers (**1**–**6**) (Fig. 1) [28–32]. Unlike pyridine (**7**, a near-oblate, asymmetric top), these isomers are highly prolate asymmetric tops with intense rotational transitions. A defining characteristic in the rotational spectra of these C_5H_5N isomers is

* Corresponding authors.
E-mail addresses: mmccarthy@cfa.harvard.edu (M.C. McCarthy), rcwoods@wisc.edu (R.C. Woods), robert.mcmahon@wisc.edu (R.J. McMahon).

https://doi.org/10.1016/j.jms.2022.111604
Received 25 January 2022; Received in revised form 5 March 2022; Accepted 7 March 2022
Available online 18 March 2022

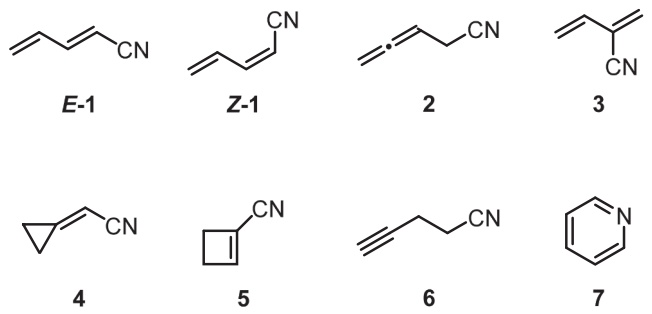

Fig. 1. C_5H_5N isomers that have been studied by rotational spectroscopy: (*E*)-1-cyano-1,3-butadiene (***E*-1**), (*Z*)-1-cyano-1,3-butadiene (***Z*-1**), 4-cyano-1,2-butadiene (**2**), 2-cyano-1,3-butadiene (**3**), (cyanomethylene)cyclopropane (**4**), 1-cyanocyclobutene (**5**), 4-cyano-1-butyne (**6**), and pyridine (**7**).

whether the vibrational ground state is 'isolated' in the frequency region of interest, which determines whether the system can be adequately fit to a single-state Hamiltonian model. Observable coupling between the ground and first fundamental states in the 130–360 GHz frequency range becomes increasingly likely when there is a vibrationally excited state that is close in energy and/or when a highly prolate species has a particularly large value of A_0 and low value of C_0. This creates a situation in which the 130–360 GHz rotational spectrum contains many transitions with very high J and K_a energy levels, allowing the ground-state energy levels to approach the vibrationally excited-state energy levels. The ground vibrational states of *s-trans-Z*-1-cyano-1,3-butadiene (***Z*-1**) [28], *syn*-2-cyano-1,3-butadiene (**3**) [31], (cyanomethylene) cyclopropane (**4**) [29], and 1-cyanocyclobutene (**5**) [32], are isolated and can be fit to a single-state, distorted-rotor Hamiltonian in the 130–360 GHz region with a low σ_{fit} value. In contrast, the ground-state rotational transitions of *s-trans-E*-1-cyano-1,3-butadiene (***E*-1**) and both conformers of 4-cyano-1,2-butadiene (**2**) [28] are not well fit by a single-state distorted rotor Hamiltonian. In the latter cases, the spectra were modeled with an effective Hamiltonian fit – a minimally perturbed, single-state, least-squares fit with exclusion of any transition frequencies that cannot be fit to a low-error distorted-rotor Hamiltonian (<50 kHz).

The open-chain isomer of pyridine presented herein, 4-cyano-1-butyne (4-pentynenitrile, **6**), has not been observed previously by rotational spectroscopy. This species is a hydrogenated version of the known interstellar molecules C_5N and HC_5N and is an ethynyl-substituted derivative of the known interstellar molecule CH_3CH_2CN. Its rotational constants were previously predicted, along with a collection of cyanodiacetylene-derived nitriles, to facilitate astronomical detection [33]. The rotational spectrum of the corresponding isonitrile (4-isocyano-1-butyne) was studied previously from 12 to 70 GHz [34], resulting in spectroscopic constants for its *anti* and *gauche* forms. The current rotational analysis of 4-cyano-1-butyne provides the first measurement, assignment, and least-squares fitting of this astrochemically intriguing species, facilitating an astronomical search and comparison to its isonitrile counterpart.

2. Computational methods

Initial electronic structure calculations of *anti*- and *gauche*-4-cyano-1-butyne were performed using Gaussian 16 [35] through the WebMO interface [36] at the B3LYP/6-311+G(2d,p) level of theory. Optimized geometries were obtained using "verytight" convergence criteria and an "ultrafine" integration grid for both energy-minimized conformers. Anharmonic vibrational frequency calculations were initially carried out using B3LYP. Although these spectroscopic constants were sufficiently accurate to begin analysis of the millimeter-wave spectrum of the *anti* conformer, they were not sufficiently accurate to begin assignment of the *gauche* conformer. (The millimeter-wave spectrum was assigned before the microwave spectrum became available). Thus, anharmonic vibrational frequency calculations were performed at the MP2/cc-pVTZ level, which provided spectroscopic constants that exhibit better agreement with the experimental constants of both conformers. A coordinate scan for the conformational analysis of the *gauche* and *anti* conformers was completed at the MP2/6-311+G(2d,p) level. A comparison of the spectroscopic constants across the B3LYP and MP2 calculations is provided in the Supplementary Material along with all other computational output files.

3. Experimental methods

A sample of 4-cyano-1-butyne was purchased commercially (Sigma-Aldrich, 97% purity), analyzed *via* ^{1}H NMR, $^{13}C\{^1H\}$-NMR, and ATR-IR spectroscopy (spectra available in Supplementary Material), and found to be sufficiently pure to be used without further refinement. A sample of 4-cyano-1-butyne at room temperature and a pressure of 6 mTorr was used to collect the 130–230 GHz and 235–360 GHz broadband spectra at the University of Wisconsin on a spectrometer described previously [24,37]. The 8–38 GHz region was collected using the same 4-cyano-1-butyne sample on a Fourier-transform microwave spectrometer at Harvard [38]. A sample of the nitrile diluted to a concentration of 0.05% in neon was supersonically expanded along the axis of a cavity-enhanced Fourier transform microwave spectrometer through a pulsed pinhole nozzle backed at 2.5 kTorr with a pulse length of 400 μs at a 6-Hz repetition rate. The spectrometer operates from 5 to 40 GHz with a line-center measurement accuracy of about 2 kHz. The large dipole moment of 4-cyano-1-butyne yielded a peak signal-to-noise ratio of the strongest transitions of about 10^2 for a 1-s integration time. The 8–38, 130–230, and 235–360 GHz segments were combined into a single broadband spectrum using Assignment and Analysis of Broadband Spectra (AABS) software [39,40]. Picket's SPFIT/SPCAT was used to conduct least-squares fitting and spectral prediction, while PIFORM, PLANM, and AC programs were used for analysis [41]. A uniform frequency measurement uncertainty of 2 kHz is assumed for all microwave measurements and 50 kHz for all millimeter-wave measurements.

4. Results

4.1. 4-Cyano-1-butyne (6)

anti-4-Cyano-1-butyne (Fig. 2a) is a highly prolate ($\kappa = -0.995$), asymmetric top (C_s) with dipole moment components predicted along the *a*- and *b*-principal axes ($\mu_a = 3.2$ D, $\mu_b = 0.84$ D; MP2/cc-pVTZ) giving rise to observable *a*- and weak *b*-type transitions. *gauche*-4-Cyano-1-butyne (Fig. 2b) is a prolate ($\kappa = -0.751$), asymmetric top (C_1) with dipole moment components predicted along each principal axis ($\mu_a = 2.0$ D, $\mu_b = 3.2$ D, $\mu_c = 0.68$ D; MP2/cc-pVTZ) creating potentially observable *a*-, *b*-, and weak *c*-type transitions. With no experimental spectroscopic constants available, the rotational constants (A_0, B_0, and C_0) of both conformers, along with their quartic and sextic centrifugal distortion constants, were calculated to facilitate initial transition assignments.

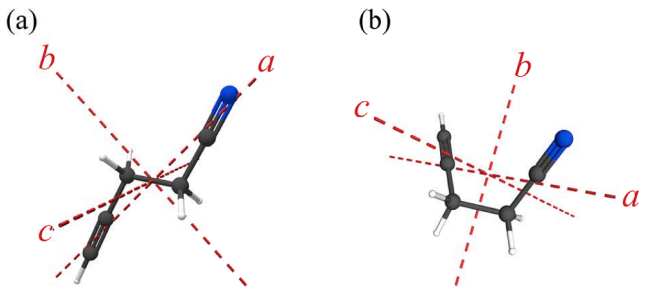

Fig. 2. 4-Cyano-1-butyne structures with principal inertial axes: (a) *anti* ($\mu_a = 3.2$ D, $\mu_b = 0.84$ D) and (b) *gauche* ($\mu_a = 2.0$ D, $\mu_b = 3.2$ D, $\mu_c = 0.68$ D).

The two energy-minimized conformations (*anti* and *gauche*) of 4-cyano-1-butyne are depicted on the conformational potential energy surface (MP2/6-311+G(2d,p)) in Fig. 3. The *gauche* conformer is predicted to be *ca.* 0.42 kcal/mol (147 cm^{-1}) higher in energy than the *anti* conformer (zero-point vibrational energy not included). This small energy difference is near the uncertainty of the level of theory employed. The rotational transition intensities of the *gauche* conformer benefit from statistical doubling due to its two enantiomeric forms. The barrier to rotation between the *gauche* and *anti* conformers (>3 kcal/mol) is sufficiently high that the transitions for each state are not expected to display observable tunneling splittings, which would increase spectral complexity and complicate the analysis. The vibrational spectra of 4-cyano-1-butyne (**6**) were observed by IR and Raman spectroscopy from 50 − 4000 cm^{-1} in the vapor, liquid, and solid states [42]. Klaeboe *et al.* note the appearance of two distinct crystalline solids at low temperature (90 K): one comprising purely the *gauche* conformers and the other purely the *anti* conformer.

4.2. Spectral analysis

Both conformations of 4-cyano-1-butyne were observed in the 8–360 GHz range with strong *a*-type R-branch bands from the *anti* conformation dominating the spectrum. The rotational spectrum of *anti*-4-cyano-1-butyne is composed of mainly $^{a}R_{0,1}$ transitions that demonstrate the typical band structure of a highly prolate, asymmetric top, in that clusters of transitions share a single *J* value. Fig. 4 shows the rotational spectrum in the 188.0–192.5 GHz range, where two such bands for the ground vibrational state of the *anti* conformer (all solid lines) can be distinguished. The $K_a = 0$ transition of the $J'' + 1 = 66$ band (magenta solid line) appears ~ 3 GHz lower in frequency within transitions of the $J'' + 1 = 65$ band. The $K_a = 1^+/1^-$ transitions are separated by 2.8 GHz, with the 1^- transition at lower frequency than $K_a = 0$ and the 1^+ transition at higher frequency. As the K_a value increases, the transitions progress to higher frequency until the first turnaround between $K_a = 2^+$ and 3^+. In this spectral window, the plus- and minus-symmetry series become degenerate at $K_a = 6$ (same values of *J* and K_a, but with values of K_c differing by one). Another turnaround is visible at $K_a = 8$, after which transitions progress to higher frequency until their transition intensities become too weak to measure. Throughout the entire frequency region, intense *b*-type R-branch transitions were observed, but only a few K_a series were of sufficient intensity to be included in the data set. No *a*-type Q- or P-branches were observed in either frequency regime, although a few sufficiently intense *b*-type, Q- and P-branch transitions were observed in the microwave region and included in the least squares fit.

The rotational spectrum of *gauche*-4-cyano-1-butyne exhibits a more typical prolate structure, wherein bands comprise transitions increasing in K_a with decreasing *J*. The bandheads are composed of quadruply degenerate *a*- and *b*-type R-branch transitions (two $^{a}R_{0,1}$ transitions, $^{b}R_{1,1}$, and $^{b}R_{-1,1}$) that share the same value of K_c. In the 188.0–192.5 GHz frequency region, transitions proceed to lower frequency as K_a increases and become non-degenerate at $K_a = 5$. The transitions progress to lower frequency and complete a turnaround many hundreds of MHz below the 188.0–192.5 GHz region. Eventually, two *a*-type transitions with the same value of K_a become a degenerate pair, while two *b*-type transitions form another set of quadruply degenerate R-branch transitions, this time with *c*-type transitions (two $^{c}R_{1,0}$ transitions, $^{b}R_{1,1}$, and $^{b}R_{1,-1}$). No *a*- or *b*-type P-branch transitions were observed for this conformer, although several series of *b*-type Q-branches were observed in the microwave region and included in the data set. No *a*-type Q branches were observed in either frequency regime.

4.3. anti-4-cyano-1-butyne ground state

The ground state of *anti*-4-cyano-1-butyne was least-squares fit to a sextic, distorted-rotor Hamiltonian with low error ($\sigma_{fit} < 50$ kHz). The experimental and predicted spectroscopic constants are reported in both

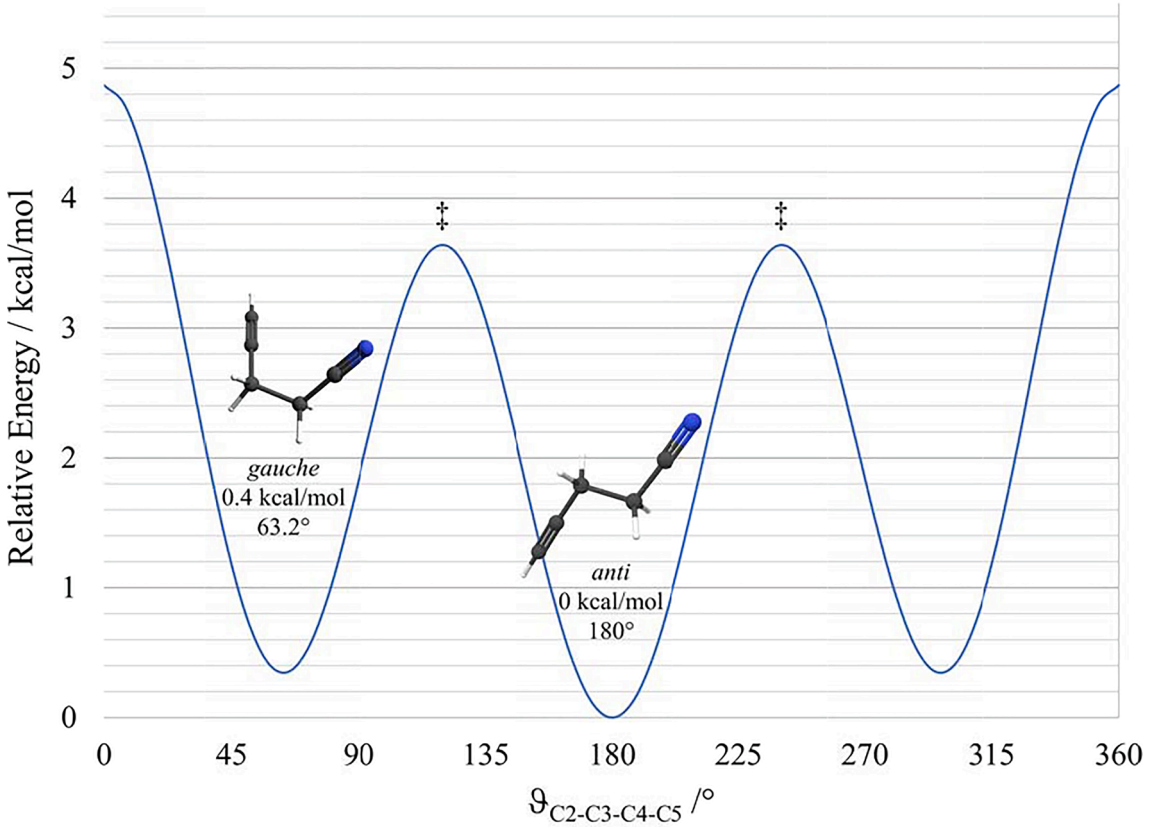

Fig. 3. Computed conformational potential energy surface of 4-cyano-1-butyne (MP2/6-311+G(2d,p)).

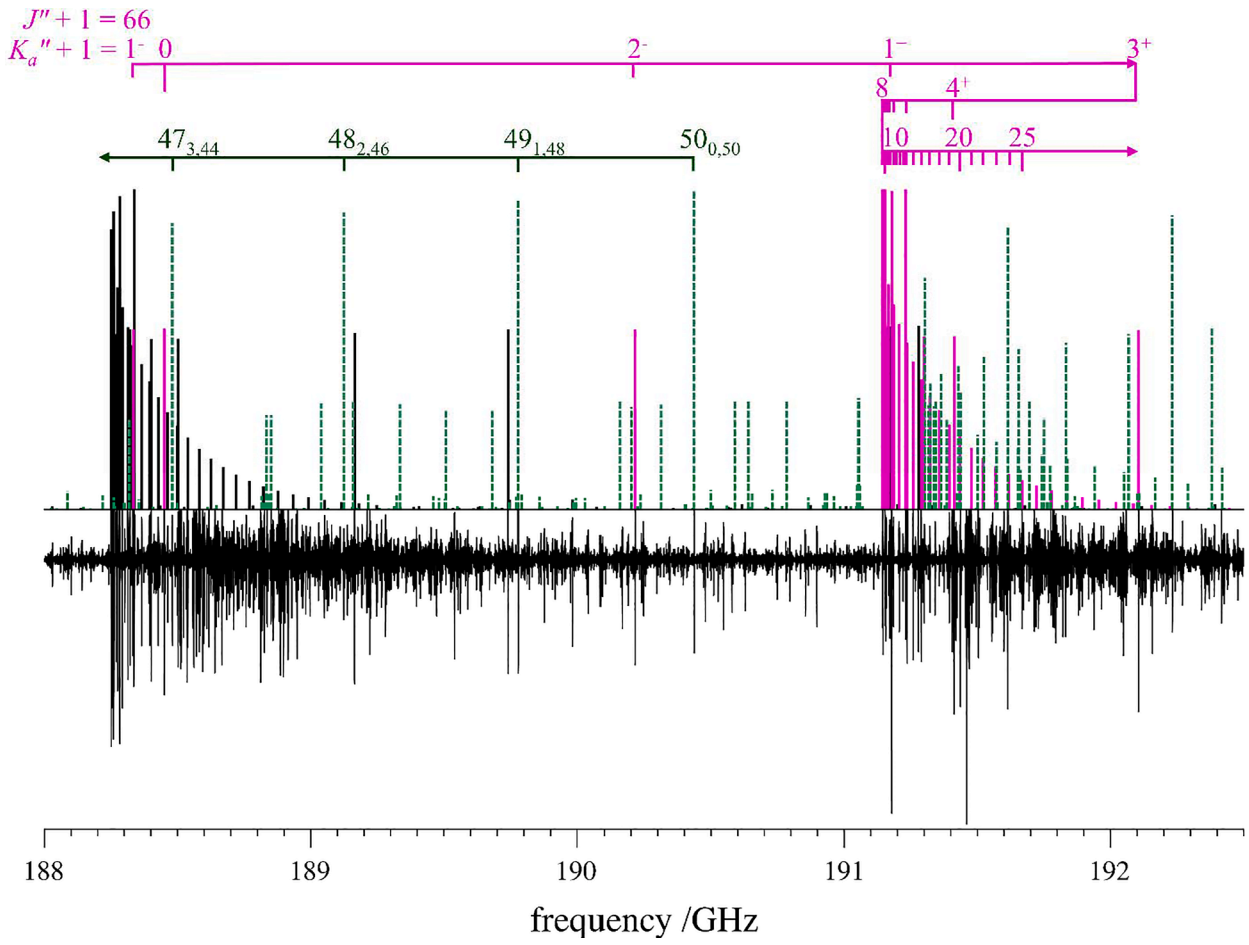

Fig. 4. Rotational spectrum of 4-cyano-1-butyne from 188.0 GHz to 192.5 GHz (bottom) and stick spectrum of the ground vibrational states (top). Dashed green lines mark transitions of *gauche*-4-cyano-1-butyne, and solid-colored lines mark transitions of *anti*-4-cyano-1-butyne. Solid lines highlighted in magenta belong to the $J'' + 1 = 66$ series of *anti*-4-cyano-1-butyne, and the corresponding $K_a'' + 1$ values are marked above. Many transitions belonging to other vibrational satellites are also visible in the experimental spectrum.

the S and A reductions, I^r representation in Table 1, and the output files for the least-squares fit are included in the Supplementary Material. In the microwave region, transitions are resolved into hyperfine multiplets that are well-predicted by the distorted-rotor model. In the millimeter-wave region, low-K_a series also demonstrate distorted-rotor behavior, but the experimental frequencies begin to subtlely deviate from those predicted at $K_a = 21$, even at the lowest J values. With increasing J, the transitions continue to further deviate from predicted frequencies until reaching a maximum deviation at $J'' + 1 = 104$. As the value of J continues to increase, transitions slowly migrate back toward their predicted distorted-rotor frequencies. A single-state, distorted-rotor model including transitions from $K_a = 0$–20 can be fit to low error ($\sigma_{fit} = 0.027$ MHz), while fits that incorporate observable transitions with $K_a > 20$ dramatically increase the error (σ_{fit}). This issue cannot be treated by inclusion of higher-order centrifugal distortion terms, making it evident that the ground state of *anti*-4-cyano-1-butyne is not amenable to a single-state, distorted-rotor Hamiltonian. It is apparent that the ground state is coupled to the lowest vibrationally excited state. Diminishing signal intensity and spectral congestion with higher-energy vibrational states make the extent to which transitions in the $K_a > 20$ series experience perturbation unclear. To obtain an effective fit for the *anti* conformer, all $K_a > 20$ transitions were excluded from the data set to allow the least-squares fit to produce minimally perturbed spectroscopic constants. Over 2,100 independent transitions were measured, including R-branch transitions with J'' values ranging from 0 to 126. The range of quantum number values for the newly measured ground-state transitions of *anti*-4-cyano-1-butyne is provided in the Fig. 5 data distribution plots.

The spectroscopic constants for the ground state of *anti*-4-cyano-1-butyne are provided in Table 1 in both the A and S reductions. The rotational constants show excellent agreement between the computed values (MP2/cc-pVTZ) and the effective experimental constants (within 0.7% for A_0, 0.3% for B_0, and 0.3% for C_0). The quartic centrifugal distortion constants are predicted by MP2 within 7.5% of the experimental values, and the sextic centrifugal distortion constants are all within 36.1%. Hyperfine-resolved transitions were not observed in the millimeter-wave region, but transitions observed in the microwave region were resolved into hyperfine multiplets arising from quadrupolar coupling to nitrogen. Experimental values of the nitrogen nuclear quadrupole coupling constants χ_{aa}, χ_{bb}, and χ_{cc} show reasonable agreement with predicted values (errors of 9.2%, 11.3%, and 7.5%, respectively). Although our analysis does not address the coupling evident in the millimeter-wave region, the agreement between the experimental and predicted constants, large number of transitions fit to low error ($\sigma_{fit} = 0.027$ MHz), and lack of obvious perturbation in the fitted series make us confident the current spectroscopic constants are physically meaningful.

Table 1
Effective experimental and predicted spectroscopic constants for the ground vibrational state of *anti*-4-cyano-1-butyne (I^r representation).

S reduction, I^r representation			A reduction, I^r representation		
	Calculated[a]	Experimental		Calculated[a]	Experimental
$A_0^{(S)}$ (MHz)	24,886	25064.23614 (34)	$A_0^{(A)}$ (MHz)	25,128	25064.23616 (34)
$B_0^{(S)}$ (MHz)	1473.0	1477.085286 (16)	$B_0^{(A)}$ (MHz)	1478.1	1477.087567 (21)
$C_0^{(S)}$ (MHz)	1415.0	1419.396089 (15)	$C_0^{(A)}$ (MHz)	1420.3	1419.393803 (20)
D_J (kHz)	0.1486	0.1501005 (14)	Δ_J (kHz)	0.1493	0.1507951 (33)
D_{JK} (kHz)	−8.209	−8.13277 (13)	Δ_{JK} (kHz)	−8.213	−8.13735 (13)
D_K (kHz)	301.8	307.79 (25)	Δ_K (kHz)	301.8	307.83 (25)
d_1 (kHz)	−0.01330	−0.0131037 (16)	δ_J (kHz)	0.01330	0.0131051 (17)
d_2 (kHz)	−0.0003219	−0.0003479 (15)	δ_K (kHz)	1.056	1.1421 (50)
H_J (Hz)	0.00007211	0.000070810 (63)	Φ_J (Hz)	0.00007357	0.00007258 (17)
H_{JK} (Hz)	−0.004470	−0.0046249 (41)	Φ_{JK} (Hz)	−0.003748	−0.0039381 (42)
H_{KJ} (Hz)	−0.06956	−0.07285 (32)	Φ_{KJ} (Hz)	−0.1034	−0.07600 (32)
H_K (Hz)	6.956	[6.956]	Φ_K (Hz)	6.958	[6.958]
h_1 (Hz)	0.00001399	0.000013003 (78)	ϕ_J (Hz)	0.00001404	0.000013048 (78)
h_2 (Hz)	0.0000007264	0.000000910 (83)	ϕ_{JK} (Hz)	0.001043	0.0061 (27)
h_3 (Hz)	0.00000005569	[0.00000005569]	ϕ_K (Hz)	0.3878	[0.3878]
χ_{aa} (MHz)[b]	−3.31	−3.6448 (36)	χ_{aa} (MHz)[b]	−3.31	−3.6448 (36)
χ_{bb} (MHz)[b]	1.43	1.6158 (17)	χ_{bb} (MHz)[b]	1.43	1.6158 (17)
χ_{cc} (MHz)[b]	1.88	2.0290 (19)	χ_{cc} (MHz)[b]	1.88	2.0290 (19)
Δ_i (uÅ^2)[c, d]	−6.24	−6.257342 (5)	Δ_i (uÅ^2)[c, d]	−6.24	−6.256241 (7)
N_{lines}[e]		128, 1994	N_{lines}[e]		128, 1994
$\sigma_{\mu\text{-wave fit}}$ (MHz)		0.0031	$\sigma_{\mu\text{-wave fit}}$ (MHz)		0.0031
$\sigma_{\text{mm-wave fit}}$ (MHz)		0.027	$\sigma_{\text{mm-wave fit}}$ (MHz)		0.027
$\sigma_{\text{total fit}}$ (MHz)		0.027	$\sigma_{\text{total fit}}$ (MHz)		0.027
$\sigma_{\text{total w.fit}}$[f]		0.587	$\sigma_{\text{total w.fit}}$[f]		0.588

[a] Evaluated at MP2/cc-pVTZ.
[b] Constants converted from the field gradient axis system to the inertial moment axis system.
[c] Inertial defect ($\Delta_i = I_c - I_a - I_b$).
[d] Calculated using PLANM from the B_0 constants.
[e] Number of independent transition frequencies for microwave and millimeter wave regions, respectively.
[f] Weighted deviation of global fits, where 2 kHz is assumed for microwave measurements and 50 kHz for millimeter-wave measurements.

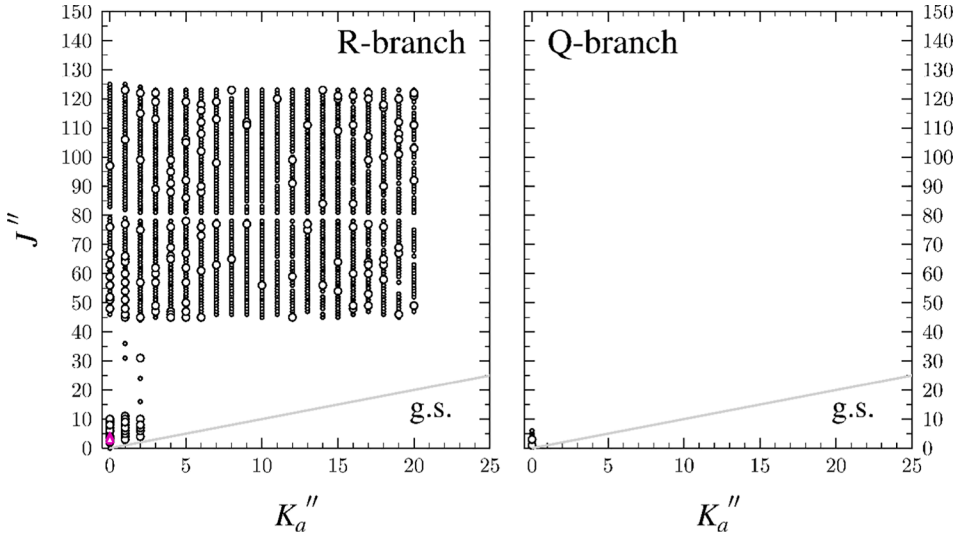

Fig. 5. Data distribution plots for the least-squares fit of spectroscopic data for the vibrational ground state of *anti*-4-cyano-1-butyne. R- and Q-branch transitions are represented by black circles, while P-branch transitions are represented as pink triangles. The size of the outlined shape is proportional to the value of $|(f_{obs.} - f_{calc.})/\delta f|$, where δf is the frequency measurement uncertainty and all values are<3.

4.4. *gauche*-4-cyano-1-butyne ground state

The *gauche* conformer was successfully identified in the millimeter-wave spectrum utilizing the MP2/cc-pVTZ predicted constants, and the assignments were confirmed by the microwave data. The microwave transitions are well-modeled by a distorted-rotor Hamiltonian, but transition frequencies begin to deviate due to coupling in the 130–360 GHz frequency region, even in the lowest K_a series. As done for the *anti* conformer, an effective fit for the *gauche* conformer was obtained by excluding transitions that deviated from distorted-rotor predicted frequencies. In the 130–360 GHz region, most quadruply degenerate transitions from K_a = 0–10 were fit to low error (σ_{fit} < 50 kHz) with distortion constants that compared reasonably (signs and orders of magnitude) with the predicted values. Including transitions with K_a > 10 resulted in a substantial increase in the error of the least-squares fit. As with the *anti* conformer, this issue cannot be treated by inclusion of higher-order centrifugal distortion terms, making it evident that the ground state of *gauche*-4-cyano-1-butyne is not amenable to a single-state, distorted-rotor Hamiltonian. Over 250 distinct transitions including *a*- and *b*-type R-branch transitions with J'' values ranging from

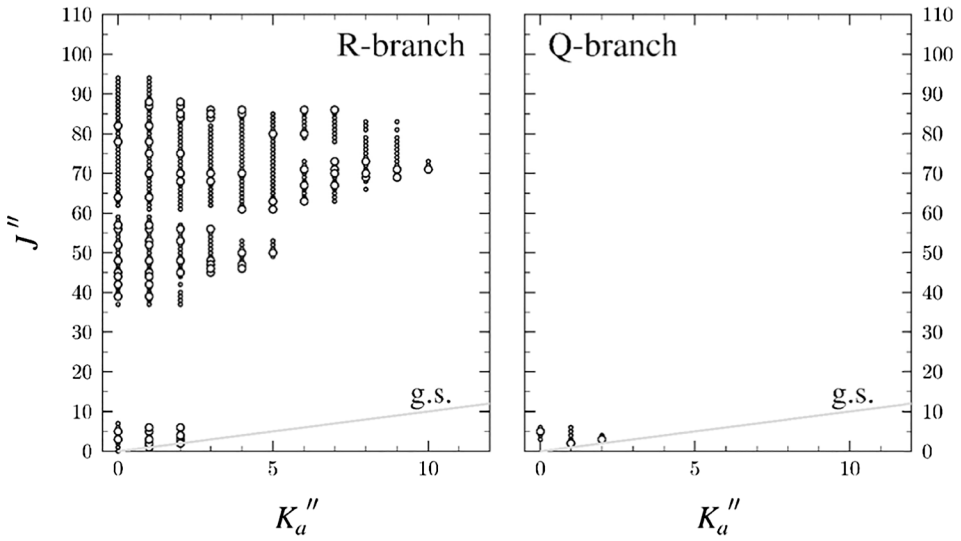

Fig. 6. Data distribution plots for the least-squares fit of spectroscopic data for the vibrational ground state of *gauche*-4-cyano-1-butyne. The size of the outlined circle is proportional to the value of $|(f_{obs.} - f_{calc.})/\delta f|$, where δf is the frequency measurement uncertainty and all values are<3.

0 to 95 and $K_a \leq 10$ were measured for the *gauche* conformer and are represented in the data distribution plot in Fig. 6.

The experimental spectroscopic constants for the ground state of the *gauche* conformer, along with the MP2-predicted constants, are reported in Table 2. In the A-reduced least-squares fit, the effective experimental rotational constants and the MP2/cc-pVTZ computed values show modest agreement (within 2.6% for A_0, 2.1% for B_0, and 0.8% for C_0), and the experimental quartic distortion constants are predicted within 12.3%. Because a limited number and type of K_a series were able to be included in the least-squares fit, some distortion terms were not well-determined. Terms Φ_{KJ} and Φ_K were held constant at their predicted values, which afforded a satisfactory fit with an error (σ_{fit}) commensurate with the experimental uncertainty. The remaining sextic centrifugal distortion constants differ substantially from their computed values. Constant Φ_{JK} has a different sign compared to the predicted value – a typical indication that a constant is absorbing coupling. There is considerable disagreement between the experimental and calculated values of the Φ_J, Φ_{JK}, and ϕ_J constants (196%, 128%, and 202%, respectively). (In the S-reduced least-squares fit, the corresponding Φ_J and ϕ_J terms are predicted within 105% and 89%, but the experimental value of Φ_{JK} differs from the prediction by almost 640%). Fixing any of these constants to their predicted value, however, massively increases

Table 2
Effective experimental and computed spectroscopic constants for the ground vibrational state of *gauche*-4-cyano-1-butyne (I^r representation).

S reduction, I^r representation			A reduction, I^r representation		
	Calculated[a]	Experimental		Calculated[a]	Experimental
$A_0^{(S)}$ (MHz)	6381	6548.45862 (12)	$A_0^{(A)}$ (MHz)	6381	6548.45742 (14)
$B_0^{(S)}$ (MHz)	2474	2422.661403 (29)	$B_0^{(A)}$ (MHz)	2474	2422.672036 (43)
$C_0^{(S)}$ (MHz)	1910	1894.290818 (15)	$C_0^{(A)}$ (MHz)	1910	1894.280311 (21)
D_J (kHz)	3.726	3.67941 (25)	Δ_J (kHz)	3.886	3.83687 (41)
D_{JK} (kHz)	−24.32	−25.7254 (43)	Δ_{JK} (kHz)	−25.28	−26.7203 (50)
D_K (kHz)	53.02	60.510 (11)	Δ_K (kHz)	53.82	61.331 (13)
d_1 (kHz)	−1.398	−1.37935 (16)	δ_J (kHz)	1.398	1.37548 (20)
d_2 (kHz)	−0.08003	−0.082600 (60)	δ_K (kHz)	4.869	5.4147 (51)
H_J (Hz)	0.02737	0.013356 (74)	Φ_J (Hz)	0.03059	0.010348 (97)
H_{JK} (Hz)	−0.1564	0.0290 (24)	Φ_{JK} (Hz)	−0.1001	0.3532 (55)
H_{KJ} (Hz)	−0.2009	[−0.2009]	Φ_{KJ} (Hz)	−0.4371	[−0.4371]
H_K (Hz)	1.231	[1.231]	Φ_K (Hz)	1.4074	[1.4074]
h_1 (Hz)	0.01409	0.007450 (34)	ϕ_J (Hz)	0.0144	0.004763 (49)
h_2 (Hz)	0.001609	0.001493 (12)	ϕ_{JK} (Hz)	0.0174	0.724 (18)
h_3 (Hz)	0.0003110	0.0003189 (18)	ϕ_K (Hz)	0.8080	1.742 (15)
χ_{aa} (MHz)[b]	0.0738	0.07500 (67)	χ_{aa} (MHz)[b]	0.0738	0.07493 (87)
χ_{bb} (MHz)[b]	−1.957	−1.84832 (19)	χ_{bb} (MHz)[b]	−1.957	−1.84807 (23)
χ_{cc} (MHz)[b]	1.884	1.77332 (85)	χ_{cc} (MHz)[b]	1.884	1.7731 (11)
Δ_i (uÅ^2)[c,d]	−18.95	−18.989536 (4)	Δ_i (uÅ^2)[c,d]	−18.95	−18.987155 (5)
N_{lines}[e]		200, 250	N_{lines}[e]		200, 250
$\sigma_{\mu\text{-wave fit}}$ (MHz)		0.0018	$\sigma_{\mu\text{-wave fit}}$ (MHz)		0.0018
$\sigma_{\text{mm-wave fit}}$ (MHz)		0.024	$\sigma_{\text{mm-wave fit}}$ (MHz)		0.024
$\sigma_{\text{total fit}}$ (MHz)		0.018	$\sigma_{\text{total fit}}$ (MHz)		0.026
$\sigma_{\text{total w.fit}}$[f]		0.557	$\sigma_{\text{total w.fit}}$[f]		0.691

[a] Evaluated at MP2/cc-pVTZ.
[b] Constants converted from the field gradient axis system to the inertial moment axis system.
[c] Inertial defect ($\Delta_i = I_c - I_a - I_b$).
[d] Calculated using PLANM from the B_0 constants.
[e] Number of independent transition frequencies for microwave and millimeter wave regions, respectively.
[f] Weighted deviation of global fits, where 2 kHz is assumed for microwave measurements and 50 kHz for millimeter-wave measurements.

the error of the least-squares fit and does not allow incorporation of many transitions into the data set. Under these circumstances, the constants represent a convolution of the effects of coupling and centrifugal distortion. As a result, the physical meaningfulness of these centrifugal distortion constants is dubious, as is the ability of the constants to predict transitions in the millimeter-wave region, where the effects of centrifugal distortion are important. With a substantial reduction in the size of the transition data set, it is not surprising that there is poorer agreement between the computed and observed spectroscopic constants. As in the *anti* conformer, hyperfine-resolved transitions were not observed in the millimeter-wave region for the *gauche* conformer, but several microwave transitions were resolved into hyperfine multiplets that were incorporated into the data set. The nitrogen nuclear quadrupole coupling constants χ_{aa}, χ_{bb}, and χ_{cc} show excellent agreement with predicted values (errors of 1.7%, 5.9%, and 6.2%, respectively). Despite the shortcomings of the current analysis – the fact that some of the spectroscopic constants differ from those predicted by MP2 and may not be physically meaningful – the analysis includes only transitions that appear to be devoid of perturbation and predicts, successfully, the highest-intensity transitions up to 360 GHz. A comparison of all predicted and experimental spectroscopic constants can be found in the Supplementary Material.

5. Conformational energy difference from relative intensity measurements

The energy difference between the *gauche* and *anti* conformers of 4-cyano-1-butyne was estimated by comparing differences in the intensities of their corresponding ground-state transitions (from 150 to 185 GHz) at 294 K [43]. The full analysis is presented in the Supplementary Material, from which we estimate an energy difference of $E_{gauche} - E_{anti} = 1.00$ (5) kcal/mol for 4-cyano-1-butyne. This energy difference is slightly larger than the predicted value (0.42 kcal/mol; MP2/cc-pVTZ) but is within range of the corresponding energy difference previously determined for the isomer, 4-isocyano-1-butyne (0.69 (14) kcal/mol) [34]. As expected, the structurally similar nitrile and isonitrile functional groups do not exhibit significantly different steric or electronic influences on the conformational equilibria.

6. Lowest excited vibrational states

The computed vibrational manifold of *anti*-4-cyano-1-butyne below 500 cm^{-1} is shown in Fig. 7(a). Given the large value of the A_0 rotational constant, the small value of the C_0 rotational constant, the predicted low energy of its vibrational states, and indications of coupling in the vibrational ground state, higher-energy vibrational states of the *anti* conformer were expected to exhibit intense coupling interactions. The C_s symmetry of the *anti* conformer and respective symmetries of the two lowest-energy excited vibrations, ν_{27} (torsion, A″, 73 cm^{-1}) and ν_{17} (in-plane bend, A', 118 cm^{-1}), allows for Coriolis coupling between the fundamental states along the *a*- and *b*- inertial axes (computed Coriolis coupling terms $G_a = 47803$ MHz, $G_b = 935$ MHz). Attempts to identify and assign ν_{27} and ν_{17} were made using the predicted vibration–rotation interaction constants (MP2/cc-pVTZ). The computed *a*-axis vibration–rotation interaction constants, however, have unusually large magnitudes and opposing signs from each other (1849.7 MHz for ν_{27} and –1784.9 MHz for ν_{17}) – a hallmark for strongly coupled states. The computed vibration–rotation interaction constants, applied to the experimental ground-state rotational constant values, did not lead to the identification of these fundamental states in the spectra. Nonetheless, the excited vibrational states of the *anti* conformer form smooth series that are visible in the Loomis-Wood plots of the ground vibrational state near $K_a = 21$. We were able to use the location of the intense bandhead transitions and the same band pattern of the ground state to assign the quantum numbers of the most intense transitions for states ν_{17} and ν_{27}. Unsurprisingly, we were unable to fit any of these states to low error using a distorted-rotor Hamiltonian, and we saw behavior indicative of intense coupling for each assignable state. A satisfactory distorted-rotor fit of even the lowest-K_a series of these vibrational states was not possible, even when using many higher-order centrifugal distortion constants. Given the observed behavior of the ground and excited vibrational states, a multistate analysis will be required to treat the perturbations in this system and obtain the spectroscopic constants of the excited vibrational states of *anti*-4-cyano-1-butyne. Such an analysis is beyond the scope of the current work. The situation for the *anti* conformer of the related isonitrile, 4-isocyano-1-butyne, is not dissimilar. Although the spectroscopic constants of the vibrational ground state appear to be free of perturbation in the measured frequency range (12–78 GHz), the vibrationally excited torsional modes show signs of

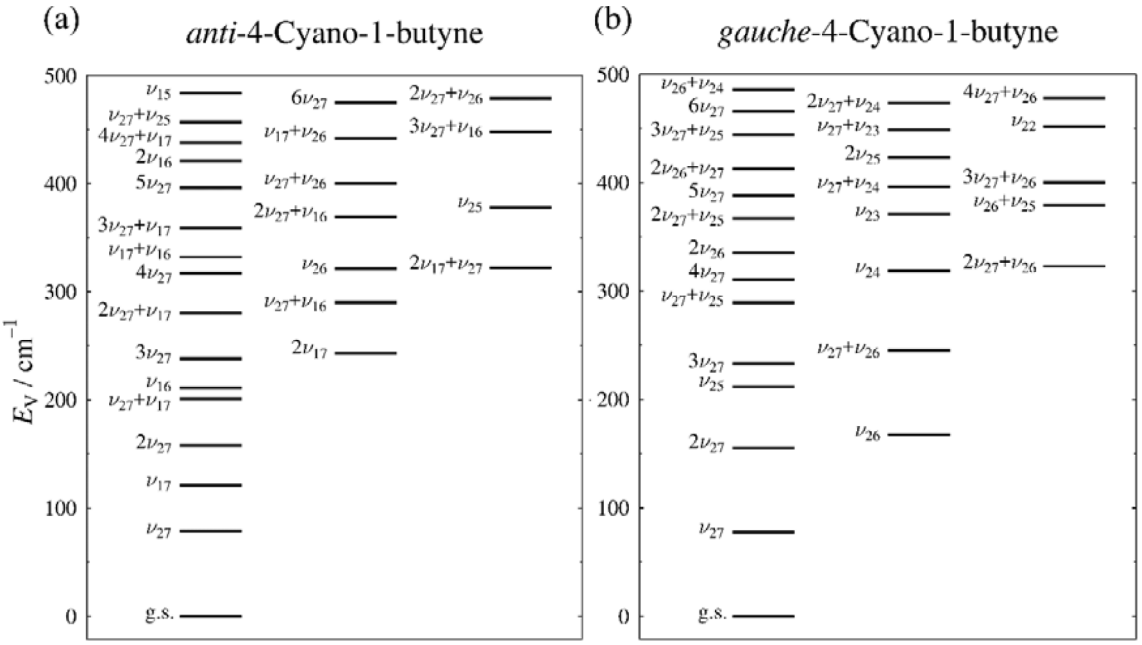

Fig. 7. Vibrational energy levels of (a) *anti*- and (b) *gauche*-4-cyano-1-butyne below 500 cm^{-1} from computed fundamental frequencies (MP2/cc-pVTZ).

unaddressed coupling [34]. The reported rotational constants do not display the expected linear relationship when plotted as a function of vibrational state [44,45].

The *gauche* conformer of 4-cyano-1-butyne exhibits a similarly complex vibrational manifold below 500 cm^{-1} (Fig. 7(b)). The predicted energies of its first two fundamental states, ν_{27} (torsion, A, 74 cm^{-1}) and ν_{26} (bend, A, 169 cm^{-1}), are low, and the vibrational manifold is comprised of many combination and overtone states. Due to the asymmetry of the *gauche* conformer (C_1), Coriolis coupling can appear between the states along all three primary axes (computed Coriolis coupling terms G_a = 4841 MHz, G_b = 205 MHz, G_c = 94 MHz). The predicted vibration–rotation interaction constants for ν_{27} and ν_{26}, along both *a*- and *b*-axes, are large in magnitude, similar in size, and opposite in sign – features indicative of coupling. Instead of using the vibration–rotation interaction constants to identify the vibrationally excited states, it was straightforward to identify transitions for the vibrationally excited states of the *gauche* conformer due to their appearance as straight series in the $K_a = 0$, Loomis-Wood plot of the vibrational ground state. Once again, we were unable to fit any of these states to low error using a distorted-rotor Hamiltonian, and we observed behavior indicative of intense coupling for each assignable state.

7. Conclusion

The ground vibrational states of both *anti*- and *gauche*-4-cyano-1-butyne show coupling to their excited states. Utilizing a Hamiltonian that models these couplings may allow the fitting of additional transitions, but would likely require assignment of many vibrational states for each conformer to completely address the spectroscopic deviations. With highly perturbed rotational spectra of astrochemically important molecules such as open-chain organic nitriles, we are often faced with choosing between a perturbation analysis involving numerous states or an effective distorted-rotor analysis to present to the spectroscopic community. Measuring substantial portions of a molecule's rotational spectrum, while avoiding inclusion of transitions that show obvious perturbation, appears to effectively model the most intense rotational transitions. While not ideal, this method may be useful in characterizing molecules likely to be sought by radioastronomers. In the current study, we generated effective fits for *anti*- and *gauche*-4-cyano-1-butyne and expect the constants presented above to enable those seeking either of these C_5H_5N conformers in harsh interstellar environments to identify them using the most intense transitions at frequencies up to 360 GHz.

Declaration of Competing Interest

The authors declare that they have no known competing financial interests or personal relationships that could have appeared to influence the work reported in this paper.

Acknowledgements

We gratefully acknowledge the National Science Foundation for support of this project (CHE-1954270, Wisconsin; AST-1908576, Center for Astrophysics). P.M.D thanks the Graduate School, University of Wisconsin-Madison, for support as an Advanced Opportunity Fellow.

Appendix A. Supplementary material

Supplementary data to this article can be found online at https://doi.org/10.1016/j.jms.2022.111604.

References

[1] H.S.P. Müller, F. Schlöder, J. Stutzki, G. Winnewisser, The cologne database for molecular spectroscopy, CDMS: a useful tool for astronomers and spectroscopists, J. Mol. Struct. 742 (2005) 215–227.
[2] H.S.P. Müller, S. Thorwirth, D.A. Roth, G. Winnewisser, The cologne database for molecular spectroscopy, CDMS, Astron. Astrophys. 370 (3) (2001) L49–L52.
[3] B.A. McGuire, A.M. Burkhardt, S. Kalenskii, C.N. Shingledecker, A.J. Remijan, E. Herbst, M.C. McCarthy, Detection of the aromatic molecule benzonitrile (*c*-C_6H_5CN) in the interstellar medium, Science 359 (6372) (2018) 202–205.
[4] B.A. McGuire, R.A. Loomis, A.M. Burkhardt, K.L.K. Lee, C.N. Shingledecker, S. B. Charnley, I.R. Cooke, M.A. Cordiner, E. Herbst, S. Kalenskii, M.A. Siebert, E. R. Willis, C.i. Xue, A.J. Remijan, M.C. McCarthy, Detection of two interstellar polycyclic aromatic hydrocarbons via spectral matched filtering, Science 371 (6535) (2021) 1265–1269.
[5] M.C. McCarthy, K.L.K. Lee, R.A. Loomis, A.M. Burkhardt, C.N. Shingledecker, S. B. Charnley, M.A. Cordiner, E. Herbst, S. Kalenskii, E.R. Willis, C.i. Xue, A. J. Remijan, B.A. McGuire, Interstellar detection of the highly polar five-membered ring cyanocyclopentadiene, Nat. Astron 5 (2) (2021) 176–180.
[6] K.L.K. Lee, P.B. Changala, R.A. Loomis, A.M. Burkhardt, C.i. Xue, M.A. Cordiner, S. B. Charnley, M.C. McCarthy, B.A. McGuire, Interstellar detection of 2-cyanocyclopentadiene, C_5H_5CN, a second five-membered ring toward TMC-1, Astrophys J. 910 (1) (2021) L2.
[7] M.C. McCarthy, B.A. McGuire, Aromatics and cyclic molecules in molecular clouds: a new dimension of interstellar organic chemistry, J. Phys. Chem. A 125 (2021) 3231–3243.
[8] K.L.K. Lee, B.A. McGuire, M.C. McCarthy, Gas-phase synthetic pathways to benzene and benzonitrile: a combined microwave and thermochemical investigation, PCCP 21 (2019) 2946–2956.
[9] J. Cernicharo, M. Agúndez, C. Cabezas, B. Tercero, N. Marcelino, J.R. Pardo, P. de Vicente, Pure hydrocarbon cycles in TMC-1: Discovery of ethynyl cyclopropenylidene, cyclopentadiene, and indene, Astron. Astrophys. 649 (2021) L15.
[10] L.W. Avery, N.W. Broten, J.M. MacLeod, T. Oka, H.W. Kroto, Detection of the heavy interstellar molecule cyanodiacetylene, Astrophys. J. 205 (1976) L173–L175.
[11] N.W. Broten, T. Oka, L.W. Avery, J.M. MacLeod, H.W. Kroto, The detection of cyanooctatetrayne (HC_9N) in interstellar space, Astrophys. J. 223 (1978) L105–L107.
[12] H.W. Kroto, C. Kirby, D.R.M. Walton, L.W. Avery, N.W. Broten, J.M. MacLeod, T. Oka, The detection of cyanohexatriyne, $H(C{\equiv}C)_3CN$, in Heiles's cloud 2, Astrophys. J. 219 (1978) L133–L137.
[13] C.M. Walmsley, G. Winnewisser, F. Toelle, Cyanoacetylene and cyanodiacetylene in interstellar clouds, Astron. Astrophys. 81 (1980) 245–250.
[14] N.W. Broten, J.M. MacLeod, L.W. Avery, W.M. Irvine, B. Hoeglund, P. Friberg, A. Hjalmarson, The detection of interstellar methylcyanoacetylene, Astrophys. J. 276 (1984) L25–L29.
[15] F.F. Gardner, G. Winnewisser, Detection of interstellar vinyl cyanide (acrylonitrile), Astrophys. J. 195 (1975) L127–L130.
[16] L.E. Snyder, J.M. Hollis, P.R. Jewell, F.J. Lovas, A. Remijan, Confirmation of interstellar methylcyanodiacetylene (CH_3C_5N), Astrophys J. 647 (1) (2006) 412–417.
[17] F.J. Lovas, A.J. Remijan, J.M. Hollis, P.R. Jewell, L.E. Snyder, Hyperfine structure identification of interstellar cyanoallene toward TMC-1, Astrophys J. 637 (1) (2006) L37–L40.
[18] P.M. Solomon, K.B. Jefferts, A.A. Penzias, R.W. Wilson, Detection of millimeter emission lines from interstellar methyl cyanide, Astrophys. J. 168 (1971) L107–L110.
[19] A. Belloche, R.T. Garrod, H.S.P. Müller, K.M. Menten, Detection of a branched alkyl molecule in the interstellar medium: *iso*-propyl cyanide, Science 345 (2014) 1584–1587.
[20] A. Belloche, R.T. Garrod, H.S.P. Müller, K.M. Menten, C. Comito, P. Schilke, Increased complexity in interstellar chemistry: detection and chemical modeling of ethyl formate and *n*-propyl cyanide in Sagittarius B2(N), Astron. Astrophys. 499 (2009) 215–232.
[21] R.A. Loomis, A.M. Burkhardt, C.N. Shingledecker, S.B. Charnley, M.A. Cordiner, E. Herbst, S. Kalenskii, K.L.K. Lee, E.R. Willis, C.i. Xue, A.J. Remijan, M. C. McCarthy, B.A. McGuire, An investigation of spectral line stacking techniques and application to the detection of $HC_{11}N$, Nat. Astron 5 (2) (2021) 188–196.
[22] M.C. McCarthy, K.L.K. Lee, P.B. Carroll, J.P. Porterfield, P.B. Changala, J. H. Thorpe, J.F. Stanton, Exhaustive product analysis of three benzene discharges by microwave spectroscopy, J. Phys. Chem. A 124 (25) (2020) 5170–5181.
[23] R.J. Halter, R.L. Fimmen, R.J. McMahon, S.A. Peebles, R.L. Kuczkowski, J. F. Stanton, Microwave spectra and molecular structures of (Z)-pent-2-en-4-ynenitrile and maleonitrile, J. Am. Chem. Soc. 123 (49) (2001) 12353–12363.
[24] M.A. Zdanovskaia, B.J. Esselman, R.C. Woods, R.J. McMahon, The 130–370 GHz rotational spectrum of phenyl isocyanide (C_6H_5NC), J. Chem. Phys. 151 (2019) 024301.
[25] M.A. Zdanovskaia, B.J. Esselman, H.S. Lau, D.M. Bates, R.C. Woods, R.J. McMahon, Z. Kisiel, The 103–360 GHz rotational spectrum of benzonitrile, the first interstellar benzene derivative detected by radioastronomy, J. Mol. Spectrosc. 351 (2018) 39–48.
[26] P.M. Dorman, B.J. Esselman, J.E. Park, R.C. Woods, R.J. McMahon, Millimeter-wave spectrum of 4-cyanopyridine in its ground state and lowest-energy vibrationally excited states, ν_{20} and ν_{30}, J. Mol. Spectrosc. 369 (2020) 111274.
[27] P.M. Dorman, B.J. Esselman, R.C. Woods, R.J. McMahon, An analysis of the rotational ground state and lowest-energy vibrationally excited dyad of 3-cyanopyridine: Low symmetry reveals rich complexity of perturbations, couplings, and interstate transitions, J. Mol. Spectrosc. 373 (2020) 111373.
[28] M.A. Zdanovskaia, P.M. Dorman, V.L. Orr, A.N. Owen, S.M. Kougias, B.J. Esselman, R.C. Woods, R.J. McMahon, Rotational spectra of three cyanobutadiene isomers

(C_5H_5N) of relevance to astrochemistry and other harsh reaction environments, J. Am. Chem. Soc. 143 (2021) 9551–9564.
[29] B.J. Esselman, S.M. Kougias, M.A. Zdanovskaia, R.C. Woods, R.J. McMahon, Synthesis, purification, and rotational spectroscopy of (cyanomethylene) cyclopropane—an isomer of pyridine, J. Phys. Chem. A 125 (25) (2021) 5601–5614.
[30] S.M. Kougias, S.N. Knezz, A.N. Owen, R.A. Sanchez, G.E. Hyland, D.J. Lee, A. R. Patel, B.J. Esselman, R.C. Woods, R.J. McMahon, Synthesis and Characterization of Cyanobutadiene Isomers – molecules of astrochemical significance, J. Org. Chem. 85 (9) (2020) 5787–5798.
[31] M.A. Zdanovskaia, B.J. Esselman, S.M. Kougias, A.R. Patel, R.C. Woods, R. J. McMahon, The 130–370 GHz rotational spectrum of *syn*-2-cyano-1,3-butadiene (C_5H_5N) – a molecule of astrochemical relevance, Mol. Phys. 119 (2021) 1964629.
[32] H.H. Smith, S.M. Kougias, B.J. Esselman, R.C. Woods, R.J. McMahon, Synthesis, purification, and rotational spectroscopy of 1-cyanocyclobutene (C_5H_5N), J. Phys. Chem. A (2022) (in press).
[33] R. Moreno, E. Silla, I. Tunon, A. Arnau, Ab initio rotational constants of the nitriles derived from cyanodiacetylene (HC_4CN), Astrophys. J. 437 (1994) 532–539.
[34] S. Samdal, H. Møllendal, J.-C. Guillemin, Microwave spectrum and conformational properties of 4-Isocyano-1-butyne ($HC{\equiv}CCH_2CH_2N{\equiv}C$), J. Phys. Chem. A 117 (40) (2013) 10304–10310.
[35] M.J. Frisch, G.W. Trucks, H.B. Schlegel, G.E. Scuseria, M.A. Robb, J.R. Cheeseman, G. Scalmani, V. Barone, G.A. Petersson, H. Nakatsuji, X. Li, M. Caricato, A.V. Marenich, J. Bloino, B.G. Janesko, R. Gomperts, B. Mennucci, H.P. Hratchian, J.V. Ortiz, A.F. Izmaylov, J.L. Sonnenberg, D. Williams-Young, F. Ding, F. Lipparini, F. Egidi, J. Goings, B. Peng, A. Petrone, T. Henderson, D. Ranasinghe, V.G. Zakrzewski, J. Gao, N. Rega, G. Zheng, W. Liang, M. Hada, M. Ehara, K. Toyota, R. Fukuda, J. Hasegawa, M. Ishida, T. Nakajima, Y. Honda, O. Kitao, H. Nakai, T. Vreven, K. Throssell, J.A. Montgomery, Jr. , J.E. Peralta, F. Ogliaro, M.J. Bearpark, J.J. Heyd, E.N. Brothers, K.N. Kudin, V.N. Staroverov, T.A. Keith, R. Kobayashi, J. Normand, K. Raghavachari, A.P. Rendell, J.C. Burant, S.S. Iyengar, J. Tomasi, M. Cossi, J.M. Millam, M. Klene, C. Adamo, R. Cammi, J.W. Ochterski, R.L. Martin, K. Morokuma, O. Farkas, J.B. Foresman, D.J. Fox, Gaussian 16 rev C.01. Gaussian, Inc., Wallingford, CT, USA, 2016.
[36] J.R. Schmidt, W.F. Polik, WebMO Enterprise, version 19.0; WebMO LLC: Madison, WI, USA, 2019. http://www.webmo.net (accessed August, 2019).
[37] B.J. Esselman, B.K. Amberger, J.D. Shutter, M.A. Daane, J.F. Stanton, R.C. Woods, R.J. McMahon, Rotational spectroscopy of pyridazine and its isotopologs from 235–360 GHz: equilibrium structure and vibrational satellites, J. Chem. Phys. 139 (2013) 224304.
[38] J.-U. Grabow, E.S. Palmer, M.C. McCarthy, P. Thaddeus, Supersonic-jet cryogenic-resonator coaxially oriented beam-resonator arrangement Fourier transform microwave spectrometer, Rev. Sci. Instrum. 76 (2005) 093106.
[39] Z. Kisiel, L. Pszczółkowski, B.J. Drouin, C.S. Brauer, S. Yu, J.C. Pearson, I. R. Medvedev, S. Fortman, C. Neese, Broadband rotational spectroscopy of acrylonitrile: vibrational energies from perturbations, J. Mol. Spectrosc. 280 (2012) 134–144.
[40] Z. Kisiel, L. Pszczółkowski, I.R. Medvedev, M. Winnewisser, F.C. De Lucia, E. Herbst, Rotational spectrum of *trans–trans* diethyl ether in the ground and three excited vibrational states, J. Mol. Spectrosc. 233 (2) (2005) 231–243.
[41] H.M. Pickett, The fitting and prediction of vibration-rotation spectra with spin interactions, J. Mol. Spectrosc. 148 (2) (1991) 371–377.
[42] P. Klaeboe, M. Moneeb, E. Törneng, H. Hopf, I. Böhm, B.N. Cyvin, S.J. Cyvin, The conformation and vibrational spectra of 1-cyano-3-butyne, Z. Naturforsch. A 35 (1980) 537–548.
[43] N. Wehres, M. Hermanns, O.H. Wilkins, K. Borisov, F. Lewen, J.-U. Grabow, S. Schlemmer, H.S.P. Müller, Rotational spectroscopy of the two conformers of 3-methylbutyronitrile (C_4H_9CN) between 2 and 400 GHz, Astron. Astrophys. 615 (2018) A140.
[44] Z. Chen, J. van Wijngaarden, The ν_{21} ring puckering mode of 3-oxetanone: a far infrared spectroscopic investigation using synchrotron radiation, J. Mol. Spectrosc. 279 (2012) 31–36.
[45] V.L. Orr, B.J. Esselman, P.M. Dorman, B.K. Amberger, I.A. Guzei, R.C. Woods, R. J. McMahon, Millimeter-wave spectroscopy, X-ray crystal structure, and quantum chemical studies of diketene: resolving ambiguities concerning the structure of the ketene dimer, J. Phys. Chem. A 120 (2016) 7753–7763.